

FEWT: Improving Humanoid Robot Perception with Frequency-Enhanced Wavelet-based Transformers

Jixin Huang^{1*}, Hanyu Liu^{1*}, Yunsheng Ma¹, Jian Shen¹, Yilin Zheng¹, Jiayi Wen¹, Baishu Wan¹, Pan Li¹, Zhigong Song^{1†}

Abstract—The embodied intelligence bridges the physical world and information space. As its typical physical embodiment, humanoid robots have shown great promise through robot learning algorithms in recent years. In this study, a hardware platform, including humanoid robot and exoskeleton-style teleoperation cabin, was developed to realize intuitive remote manipulation and efficient collection of anthropomorphic action data. To improve the perception representation of humanoid robot, an imitation learning framework, termed *Frequency-Enhanced Wavelet-based Transformer* (FEWT), was proposed, which consists of two primary modules: *Frequency-Enhanced Efficient Multi-Scale Attention* (FE-EMA) and *Time-Series Discrete Wavelet Transform* (TS-DWT). By combining multi-scale wavelet decomposition with the residual network, FE-EMA can dynamically fuse features from both cross-spatial and frequency-domain. This fusion is able to capture feature information across various scales effectively, thereby enhancing model robustness. Experimental performance demonstrates that FEWT improves the success rate of the state-of-the-art algorithm (*Action Chunking with Transformers*, ACT baseline) by up to 30% in simulation and by 6-12% in real-world.

I. INTRODUCTION

In the field of imitation learning [1], humanoid robot learning effectiveness is usually determined by the quality and diversity of expert demonstrations and the perception representations. Proprioceptive information primarily includes action sequences and sensor feedback. Meanwhile, the robot's perception of the external environment is equally important, and sensing the environment through RGB images is the dominant approach. Visual representations primarily reflect environmental image information in robot learning. Despite substantial advances in computer vision, learning robust and generic visual representations suitable for robotic applications remains a significant challenge [2][3]. Vision system design should prioritize optimizing model architectures and vision representations over merely increasing dataset size [3]. Existing attention mechanisms effectively enhance feature representation, e.g., the *Efficient Multi-Scale Attention* (EMA) [4] module excels in target detection and is well-suited for improving the visual representation of robots. Incorporating the EMA module into a backbone network (e.g., ResNet [5]) improves multi-scale feature representation within the model. However, EMA module focuses only on cross-spatial feature

enhancement, neglecting frequency-domain information. To address this limitation, wavelet transform can be integrated to improve the comprehensiveness of feature representation. Wavelet transform is a powerful tool for capturing frequency-domain features, with the Discrete Wavelet Transform (DWT) being widely used in vision tasks due to its ability in Multiresolution Analysis. HWD [6] emphasized that Haar wavelet down sampling improves the performance of semantic segmentation models by preserving key information. SFFNet [7] integrates spatial and frequency domain information using the Haar wavelet transform to enhance performance in remote sensing image segmentation, particularly in complex scenes. The wavelet transform in the WF-Diff [8] framework enhances underwater image quality by decomposing the image into low-frequency and high-frequency components, reducing color degradation and detail loss, and achieves competitive performance in visual quality.

To enhance the feature representation of the EMA module, we propose the *Frequency-Enhanced Efficient Multi-Scale Attention* (FE-EMA) module, which is plug-and-play. By introducing the frequency-domain enhancement mechanism and combining it with wavelet transform, FE-EMA achieves a balanced consideration of both cross-spatial and frequency-domain features. This approach effectively enhances the comprehensiveness of model feature representation. In addition, capturing time-series and channel features can enhance the predictive performance of the model. For example, FECAM [9] introduces a *Frequency Enhanced Channel Attention Mechanism* (FECAM) using the Discrete Cosine Transform, which effectively combines time-domain and frequency-domain features, significantly improving the prediction performance of time-series models. Inspired by the FECAM framework, we integrate the DWT into time-series modeling to enable more effective multi-scale decomposition of temporal data, thereby enhancing the model's ability to capture rich temporal features for accurate prediction. Additionally, the integration of inertial measurement unit (IMU) data from the mobile chassis with humanoid robot joint positions further enhances perception abilities.

In the experimental analysis, we employ the *Gradient-weighted Class Activation Mapping* (Grad-CAM) [10] visualization technique to analyze the regions of interest in the deep neural network. Comparing heat maps to visualize key areas of model focus enhances the understanding of decision-making mechanisms. Experimental results show that FEWT significantly outperforms the original baseline policy of *Action Chunking with Transformers* (ACT) [11], improving the task success rate.

The main contributions and work in this paper are as follows:

*These authors contributed equally to this work.

†Corresponding author: song_jnu@jiangnan.edu.cn.

¹Jiangsu Provincial Key Laboratory of Food Advanced Manufacturing Equipment Technology, School of Mechanical Engineering, Jiangnan University, Wuxi 214122, China. This work was supported by the National Natural Science Foundation of China (Grant No. 12202159, 12472216) and the Wuxi Taihu Lake Talent Plan.

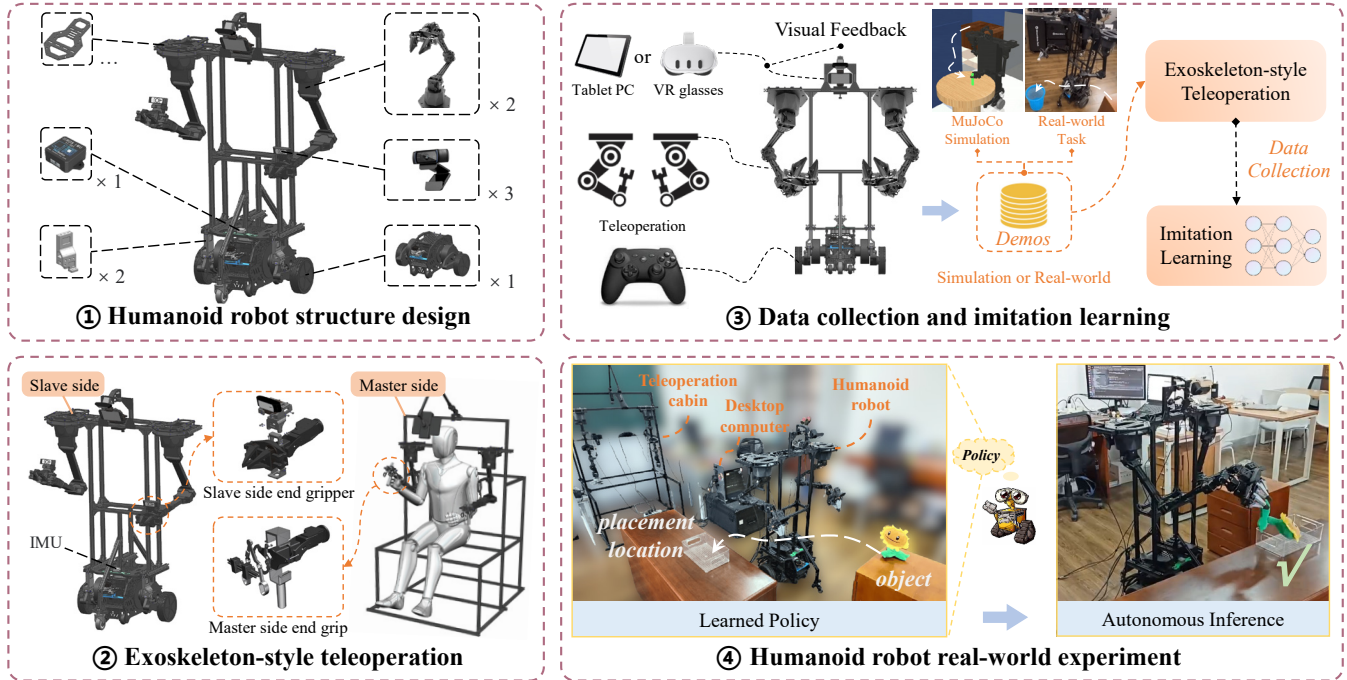


Fig. 1: We have developed a low-cost humanoid robot platform. The humanoid robot collects data through exoskeleton-style teleoperation. It performs complex tasks, such as transferring a doll between the left and right hands and placing it into a storage box, using imitation learning.

1) We developed the *Humanoid Black Knight* (HBK) hardware platform to support imitation learning research and the deployment of humanoid robot algorithms (see **Fig. 1**). Anthropomorphic data collection from the humanoid robot arms was accomplished using exoskeleton-style teleoperation, ensuring natural interaction and precise motion mapping;

2) We propose an innovative model training framework: the *Frequency-Enhanced Wavelet-based Transformer* (FEWT). It mainly consists of two modules: FE-EMA and *Time-Series Discrete Wavelet Transform* (TS-DWT);

3) The superiority of the FE-EMA module in feature extraction and visual representation is validated through ablation experiments in the MuJoCo [12] simulation. Additionally, the effectiveness of the TS-DWT network in optimizing the Transformer [13] architecture is demonstrated, as shown in Ablation Experiment **Table III**. The comparative experiments demonstrate that FEWT outperforms current mainstream robotic learning methods in both simulation and real-world experiments, as shown in **Table IV** and **Table V**.

II. RELATED WORKS

A. Robot Teleoperation Data Collection

The datasets for imitation learning primarily consist of expert demonstrations generated through teleoperation. Teleoperation enables real-time cross-space manipulation by incorporating humans into the control loop, where humans make decisions and robots perform physical actions [14][15]. Currently, mainstream teleoperation schemes include joint mapping [11][16], motion retargeting [17][18], end position control [19], and VR control [20][21][22], etc. The *ALOHA* [11][16] adopts a joint mapping technique, which enables

teleoperation by directly mapping the joint positions of the master arm to those of the slave arm. Exoskeleton equipment improved manipulation accuracy and user experience through real-time mapping and joint feedback information [23][24]. For example, TABLIS [24], a seat-type whole-body exoskeleton cockpit developed by the University of Tokyo, enables bilateral teleoperation of humanoid robots to overcome the space limitation of movement. The AirExo [25] exoskeleton equipment developed by Shanghai Jiao Tong University is used for data collection in imitation learning of robotic dual-arm systems, supporting joint-level teleoperation as well as learning of whole-arm manipulation in the wild. The ACE [26] teleoperation system, developed by the University of California, San Diego, is a low-cost, cross-platform visual-exoskeletons teleoperation system. This exoskeleton supports high-precision teleoperation and aids imitation learning across various platforms.

B. Robot Skill Learning

Currently, the skill learning algorithms are widely applied in autonomous robots, including Google RT series, which generates action sequences using the Transformer [13] architecture; Diffusion Policy [27], which creates action sequences through diffusion process modeling; and ACT [11][16] imitation learning series, which trains models using expert demonstration data to perform autonomous tasks. Each approach has unique characteristics and provides significant impetus for developing intelligent robot manipulation in embodied intelligence [28]. RT-1 [29] enables efficient multimodal task execution by annotating images, texts, and actions using the Transformer architecture and imitation learning with linguistic conditioning. RT-2 [30] enhances the

system generalization ability by integrating a Large Language Model and environmental understanding. To meet the data requirements of the Large Language Model in robot learning, Google created RT-X [31] for building a large-scale comprehensive dataset. Diffusion Policy [27] applies the Diffusion Model [32] for action generation in robotics. Diffusion Policy enables achieving action generation by modeling the visual action policy as a conditional denoising and diffusion process. The method effectively expresses complex multimodal action distributions and demonstrates strong generalization ability, but the high computation limits real-time image processing, which remains the main bottleneck in robot policy applications.

The ACT Policy implemented in the *ALOHA* has become a benchmark in robot learning for robotic manipulation via imitation learning. *ALOHA* is available in two versions: static desktop (*Static ALOHA* [11]) and dynamic mobile (*Mobile ALOHA* [16]). *Static ALOHA* is a dual-armed system fixed to a tabletop, designed for performing various fine-grained desktop tasks; *Mobile ALOHA* integrates a mobile chassis for whole-body manipulation tasks in dynamic environments. *Static ALOHA* is equipped with four RGB cameras to capture visual information about the environment. The ACT policy uses joint positions and RGB images as conditional inputs, combining Convolutional Neural Networks (CNN) with Conditional Variational Autoencoders (CVAE), allowing the system to use the current image as a task command to guide robot action decisions. Intuitively, ACT attempts to imitate a human operator by predicting actions in the next time step based on the current observed situation. The observation space

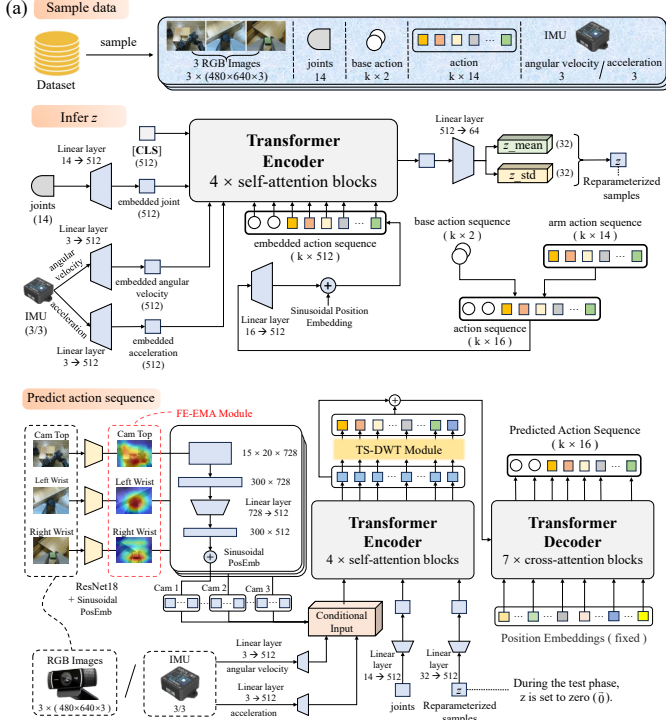


Figure 2: The model framework of the Frequency-Enhanced Wavelet-based Transformer (FEWT). (a) Detail architecture of the FEWT; (b) Network architecture of the Frequency-Enhanced Efficient Multi-Scale Attention (FE-EMA) module; (c) Network architecture of the Time-Series Discrete Wavelet Transform (TS-DWT) module.

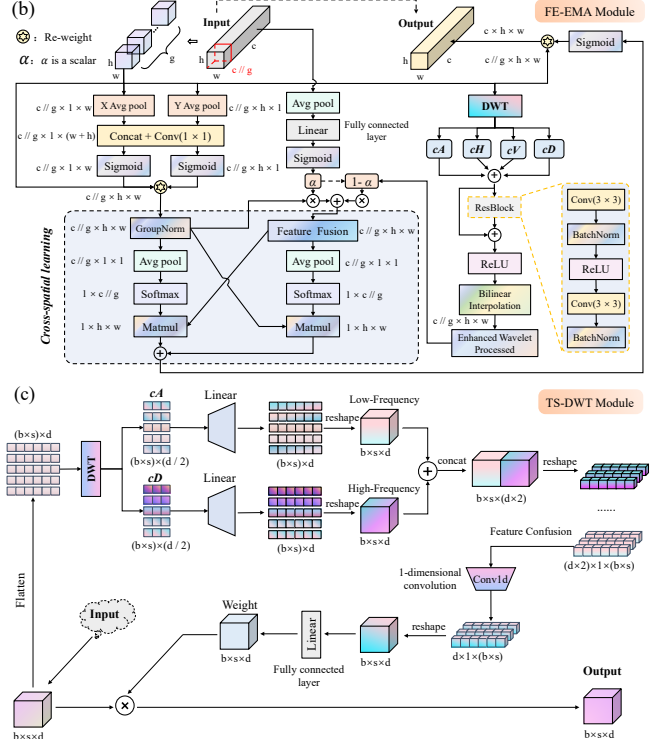
includes a 480×640 image and the current joint positions for both robots. The control frequency of the robot is 50HZ.

III. SYSTEM DESCRIPTION

A. Humanoid Robot Hardware Design

The humanoid robot we designed is named *Humanoid Black Knight* (HBK). The construction of HBK mainly consists of two 7-dof (arm + gripper) robotic arms (*ViperX-300*) [33], a two-wheeled differential mobility chassis (*Diablo*) [34], three RGB cameras (Logitech C922x webcams), and an inertial measurement unit (IMU). The top is equipped with a visual feedback screen and a camera to monitor the bimanual manipulation. The remote visual feedback can be provided through multi-view observation using a Tablet PC or VR glasses (see Fig. 1 ③).

Referring to the joint mapping teleoperation scheme used in *ALOHA* [11][16] system, we invert the robotic arm at the master-slave end and use a remote screen with visual feedback. By using exoskeleton-style teleoperation to collect expert demonstration data, we achieve high-precision manipulation, and more natural and effective teleoperation for humanoid robots. Compared to the conventional dual-arm base link layout design of *Mobile ALOHA*, the dual-arm inverted design of HBK is more anthropomorphic in appearance and more natural in manipulation. For data collection of the humanoid robot's specific skill, it is sufficient to collect about 25 to 50 sets of expert demonstrations [16]. Remote manipulation master-slave control in data collection is achieved through *Robot Operating System* (ROS).



B. The model framework of FEWT

In humanoid robot learning, visual representation directly affects the task execution ability by extracting environmental information features, achieving perception, decision-making, and action planning. To enhance the humanoid robot's visual representation, we introduce the FE-EMA module to achieve a balanced fusion of both cross-spatial and frequency-domain information, motivating the proposal of the *Frequency-Enhanced Wavelet-based Transformer* (FEWT) framework. The model framework of FWT is shown in **Fig. 2**.

Building on the baseline model of ACT Policy, a model framework for FWT was developed and trained as a Conditional Variational Autoencoder (CVAE), consisting of an encoder and a decoder. FWT mainly consists of two modules, FE-EMA and TS-DWT. The encoder of the CVAE compresses the action sequences, the joint observations, and the IMU data into the “style variable” z . The CVAE decoder predicts a series of actions based on images from three different views. The decoder generates action sequences from images of three views, joint positions, IMU data, and z using the Transformer encoder. It then predicts actions through the Transformer decoder. In the testing phase, z is simply set to the mean of the prior (i.e., zero). In this case, the IMU data of the moving chassis contains the linear velocity and acceleration. Integrating IMU data into the model training process optimizes motion control accuracy of the mobile chassis. It also improves the performance of the humanoid robot in dynamic environments by providing precise linear velocity and acceleration information (see **Table V**). In **Fig. 2(a)**, “ k ” denotes the length of the target action sequence in the demonstration dataset.

C. Frequency-Enhanced Efficient Multi-Scale Attention

FE-EMA module implements two key improvements based on the EMA [4] module:

(1) Frequency-domain Enhancement: capturing multi-scale feature through wavelet transform to enhance the richness of feature representation;

(2) Adaptive Fusion: dynamically adjusting the fusion ratio of the cross-spatial and frequency-domain features by using the weighting parameter α to effectively enhance the robustness and adaptability of the model.

Given an input feature map X , its wavelet transform represents the signal as **Equation (1)** by constructing a set of scaled and translated wavelet basis functions $\psi_{j,k}(x)$ and scale functions $\phi_{j,k}(x)$.

$$X = \sum_{j \in Z} \sum_{k \in Z} \left(cA_{j,k} \cdot \phi_{j,k}(x) + \sum_{i=1}^3 cD_{i,j,k} \cdot \psi_{i,j,k}(x) \right) \quad (1)$$

Where j is the scale parameter, which controls the frequency resolution. k is the translation parameter, which controls the spatial-temporal localization. $cA_{j,k}$ is the low-frequency approximation coefficient. $cD_{i,j,k}$ is the high-frequency detail coefficient, which captures the details in the horizontal, vertical, and diagonal directions, respectively. Z denotes the set of integers, i.e., all integers, which is used to indicate that the variables j and k can take on any integer value.

On a 2D feature map X , the wavelet transform can be implemented using a 2D filter bank. The wavelet decomposition of the feature map by rows and columns respectively yields the following coefficients: $DWT(X) = (cA, cH, cV, cD)$. Where cA denotes the low-frequency approximation component, capturing the overall structural information. cH denotes the horizontal detail component, capturing the horizontal edge features. cV denotes the vertical detail component, capturing the vertical edge features. cD denotes the diagonal detail component, capturing the edge variations in the diagonal direction.

The convolution kernel of Haar wavelet is defined in **Equation (2)**, where L is the low-pass filter, which is used for the extraction of low-frequency components. H is a high-pass filter for extracting high-frequency components.

$$L = \frac{1}{\sqrt{2}} [1 \ 1]^T, \quad H = \frac{1}{\sqrt{2}} [1 \ -1]^T \quad (2)$$

DWT decomposes the feature map into frequency components and reduces size, while subsequent convolutions focus on low-dimensional features to improve efficiency. Meanwhile, FE-EMA uses grouped convolution to process only the down-sampled features. This approach can reduce computation (FLOPs) and improve model performance and efficiency. **Table I** shows that, based on the ACT Policy baseline and Backbone (ResNet18), the FE-EMA reduces the computational complexity (FLOPs) compared to the EMA. The Simulation Tasks are **Cube Transfer** and **Bimanual Insertion**, respectively (see **Table II**).

In the FE-EMA module, dynamic weights α are used to control the fusion of cross-spatial and frequency-domain features. The weights α are generated by global average pooling and a linear layer: $\alpha = \sigma(W \cdot GAP(X))$, where $\sigma(\cdot)$ is the Sigmoid function, GAP is the global average pooling, and the weight matrix W is linearly transformed on this feature vector to learn the weight assignments of the features.

The spatial and frequency-domain fused feature X_{fused} is shown in **Equation (3)**. Ultimately, the module generates a cross-space attention map using matrix dot product. This accurately captures pixel-level relationships and enhances feature representation.

$$X_{fused} = \alpha \cdot X_{spatial} + (1 - \alpha) \cdot X_{fre} \quad (3)$$

$X_{spatial}$ in **Equation (3)** is a spatial feature generated through the attention mechanism and group normalization process. It is combined with the frequency-domain feature X_{fre} to ensure a more comprehensive information capture of the model at multiple scales. The network architecture of the FE-EMA module is shown in **Fig. 2(b)**.

TABLE I. COMPARISON OF PARAMETERS AND FLOPS FOR ONE EPOCH

Method	Backbone	Simulation Tasks	
		#.Param.	FLOPs
Baseline (ACT [11])	ResNet18	60.7566 M	37570.51 M
EMA + ACT		60.7592 M	37616.59 M
FE-EMA + ACT (ours)		60.7621 M	37596.91 M

D. Time-Series Discrete Wavelet Transform

The application of DWT in image processing is well established. However, its potential for time-series data modeling has not been fully explored. Similar to images, time-series data contain rich, multi-scale features, and the decomposition and reconstruction abilities of DWT offer new possibilities for time-series modeling. Therefore, building on the successful application of the DWT in image processing, this work incorporates DWT into time-series analysis. This integration can enhance the ability of predictive models to accurately capture multi-scale features.

The network architecture of the TS-DWT module is shown in **Fig. 2(c)**. After inputting the time-series tensor, the tensor is first decomposed using DWT to extract the low-frequency component (cA) and the high-frequency component (cD). Subsequently, cA and cD are upscaled and spliced by a linear layer. Next, the spliced low-frequency and high-frequency components are feature fused using Conv1d, and then the frequency-domain attentional weights are computed by the fully connected layer. Finally, the frequency-domain attention weights are multiplied with the input time-series tensor to output the frequency-domain tensor.

TABLE II. SUMMARY OF TASK-SPECIFIC DATASETS AND PHASES FOR ROBOTIC MANIPULATION IN ACT SIMULATION BASELINE

Dataset	Phase1	Phase2	Phase3	Length	Num	Total size
<i>Cube Transfer</i> (sim)	Touched	Lifted	Transfer	400	50	18.4G
<i>Bimanual Insertion</i> (sim)	Grasp	Contact	Insert	400	50	18.4G

TABLE III. COMPARISON OF SUCCESS RATE (%) FOR ACT SIMULATION TASKS IN ABLATION EXPERIMENT

Method	<i>Cube Transfer</i> (sim)			<i>Bimanual Insertion</i> (sim)		
	Touched	Lifted	Transfer	Grasp	Contact	Insert
Baseline (ACT [11])	97	90	86	93	90	32
EMA [4] + ACT	98	96	96	92	90	40
FE-EMA + ACT (ours)	100	100	100	94	94	58
TS-DWT + ACT (ours)	100	98	98	96	92	42
EMA + TS-DWT + ACT	98	96	96	92	90	36
FE-EMA + TS-DWT + ACT (ours: FEWT)	100	98	98	96	94	62

IV. EXPERIMENT AND ANALYSIS

A. Ablation and Comparative Experiment

Based on MuJoCo [12] simulation, the learning effect of the FEWT model is verified through simulation experiments. The dataset generated by the simulation task contains 50 sample sets, with all data uniformly stored in HDF5 file format. The object initialization positions for each simulation task are randomly generated within a given interval.

The dataset in **Table II** contains only the top camera view (Top Image). Length denotes the overall time step for the simulation task, with delay time $DT = 0.02$ seconds between each time step (control frequency of 50Hz). “Num” denotes the number of samples in the dataset, and “Total size” denotes the overall memory size of the dataset in Gigabytes (G).

A summary of the specific data from the ablation experiments is given in **Table III**. After the model training was completed, 50 tests were conducted for each simulation task. The experimental results show that FEWT significantly outperforms the ACT original baseline policy in terms of simulation task success rate. FEWT can increase the success rate of the ACT baseline in simulation by up to 30%. **Table IV** and **Table V** present a comparative experiment between FEWT and existing mainstream robot learning algorithms.

B. Grad-CAM Visualization

In deep learning, understanding how the model perceives the data is critical. *Gradient-weighted Class Activation Mapping* (Grad-CAM) is a visualization technique. Grad-CAM uses gradient information from the CNN to generate a heat map, highlighting the regions that contribute most to the prediction results and visually demonstrating the model’s decision basis. This approach helps researchers verify the correctness of model decisions and can also be used for model interpretability. For two different simulation tasks (ACT [11] baseline), **Cube Transfer** and **Bimanual Insertion**, Top Image is visualized and compared and analyzed using Grad-CAM. From **Fig. 3(a)** and **Fig. 3(b)**, it can be observed that the model’s ability to focus is significantly better than the baseline model after introducing the FE-EMA module in ResNet18, the backbone network of ACT. This improvement is key to the significant increase in the success rate of the simulation task.

Fig. 3(c) and **Fig. 3(d)** present a comparative analysis of the *Building blocks* (sim) and *Doll Storage* (real) task (Top Image) visualization using Grad-CAM, applied to the humanoid robot experiment. In the heatmap, the red areas represent the regions where the model focuses its attention.

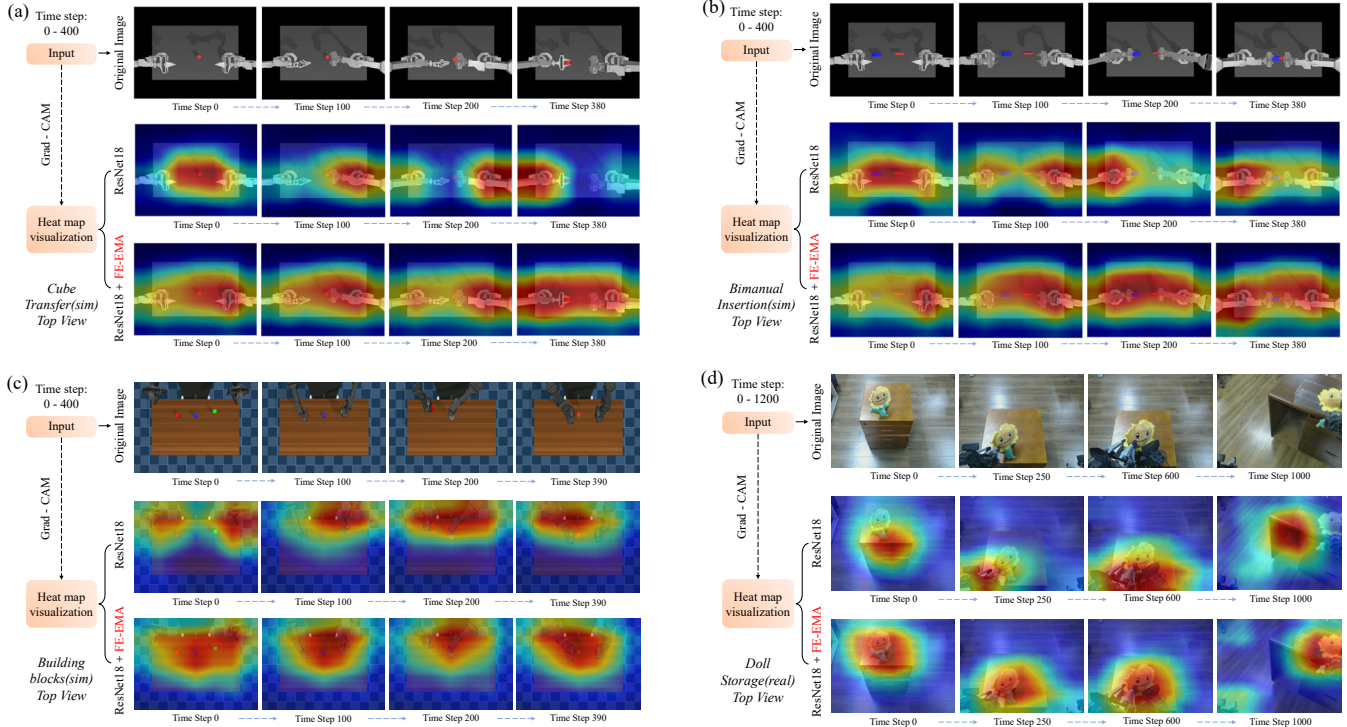


Fig. 3: Comparison of Heat map Visualizations for the simulation and real-world Task. Grad-CAM was utilized to visualize the model’s attention regions, specifically for top view images. (a) **Cube Transfer** (sim); (b) **Bimanual Insertion** (sim); (c) **Building blocks** (sim); (d) **Doll Storage** (real).

TABLE IV. SUMMARY OF TASK-SPECIFIC DATASETS AND PHASES FOR ROBOT MANIPULATION IN SIMULATION AND REAL-WORLD

Dataset (sim / real)	Phase1	Phase2	Phase3	Length	Num	Total size	Success rate (ACT)	Success rate (FEWT)
<i>Building blocks</i> (sim)	grasp	place	place	400	50	51.5G	94%	96%
<i>Drawer Storage</i> (sim)	grasp	lifted	place	400	50	51.5G	94%	100%
<i>Lifted Curtain</i> (sim)	lifted	grasp	place	350	50	45G	84%	92%
<i>Strip Transfer</i> (sim)	grasp	lifted	place	300	50	38.6G	96%	100%
<i>Charm Splicing</i> (real)	lifted	approach	splicing	800	20	41.2G	92%	98%
<i>Throw Paper</i> (real)	reach	grasp	place	1000	25	64.4G	86%	94%
<i>Drawer Storage</i> (real)	reach	opened	place	1200	25	77.2G	74%	84%
<i>Doll Storage</i> (real)	reach	transfer	place	1200	25	77.2G	70%	82%

TABLE V. A COMPARATIVE EXPERIMENT ON THE SUCCESS RATES OF DIFFERENT ROBOT LEARNING POLICY

Policy	<i>Building blocks</i> (sim)	<i>Drawer Storage</i> (sim)	<i>Lifted Curtain</i> (sim)	<i>Strip Transfer</i> (sim)	<i>Charm Splicing</i> (real)	<i>Throw Paper</i> (real)	<i>Drawer Storage</i> (real)	<i>Doll Storage</i> (real)
DP (DDPM) [27]	80	76	82	80	74	70	68	60
DP (DDIM) [16]	88	84	90	86	88	80	76	72
ACT [11]	94	94	84	96	92	86	74	70
FEWT (without IMU)	96	100	92	100	98	90	80	76
* FEWT (with IMU)	—	—	—	—	98	94	84	82

* No chassis motion is involved in simulation; “—” indicates not evaluated.

C. Humanoid Robot Experiment and Analysis

The superiority of the FEWT framework was verified through ablation experiments, followed by testing the skill learning of the humanoid robot (HBK) using the FEWT model. **Table IV** summarizes the data of the humanoid robot in different simulated and real-world tasks. It compares the performance of the ACT and FEWT models in terms of task

success. After the model training was completed, 50 tests were conducted for each task. The results show that FEWT (with IMU) can improve the ACT baseline by 6-12% in real-world mobile bimanual manipulation tasks.

To highlight the advantages of the FEWT model in robot manipulation task success rates, this study selects mainstream robotic learning algorithms such as ACT [11] and Diffusion Policy [16], [27], and conducts comparative analysis of their

performance in task completion success rates through both simulation and real-world experiments. Overall, the FEWT outperforms the existing mainstream methods, demonstrating superior performance. Detailed algorithm comparison results can be found in **Table V**.

Fig. 4 shows the static desktop skill learning screen of the HBK in the MuJoCo simulation environment, along with the camera view for data collection of different mobile tasks in a real-world scenario.



Fig. 4: Static desktop skill learning in the MuJoCo simulation environment with a camera view of data collection in the real-world. (a) *Building Blocks* (sim); (b) *Drawer Storage* (sim); (c) *Lifted Curtain* (sim); (d) *Strip Transfer* (sim); (e) *Throw Paper* (real); (f) *Charm Splicing* (real); (g) *Drawer Storage* (real); and (h) *Doll Storage* (real).

We deploy our policy with inference on a desktop with an NVIDIA RTX 3060 GPU. **Fig. 5** illustrates the effect of HBK autonomous learning manipulation in various real-world tasks, demonstrating the reliability and robustness of the FEWT model across these tasks. Using FEWT enables whole-body coordinated control and autonomous mobile manipulation of humanoid robots in complex environments, enhancing the adaptability and execution ability of the robots in dynamic tasks.

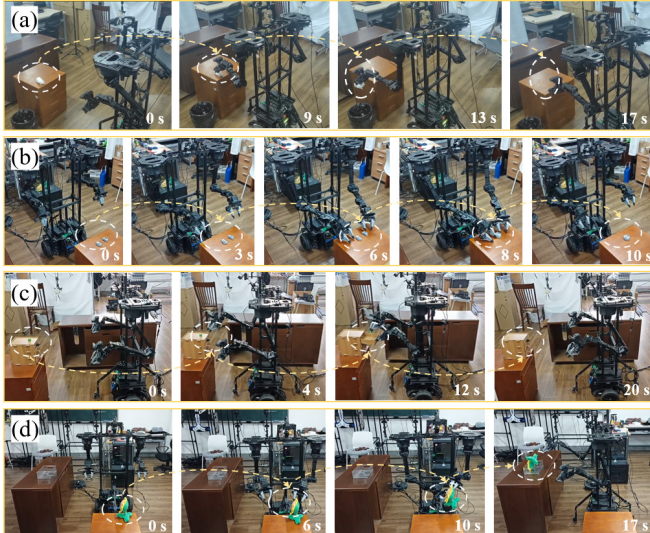


Fig. 5: Demonstration of skill learning by humanoid robot autonomous skills in the real-world. (a) *Throw Paper*; (b) *Charm Splicing*; (c) *Drawer Storage*; (d) *Doll Storage*.

For the ACT simulation tasks, ***Cube Transfer*** and ***Bimanual Insertion***, changes in the dynamic weights α of the FE-EMA module during training are shown in **Fig. 6**. This suggests that the cross-spatial and frequency-domain feature

weights are well balanced during network model training. The quantitative analysis of dynamic weight variations demonstrates that parameter α can adaptively fuse cross-spatial and frequency-domain features, enabling the effective capture of multi-scale information.

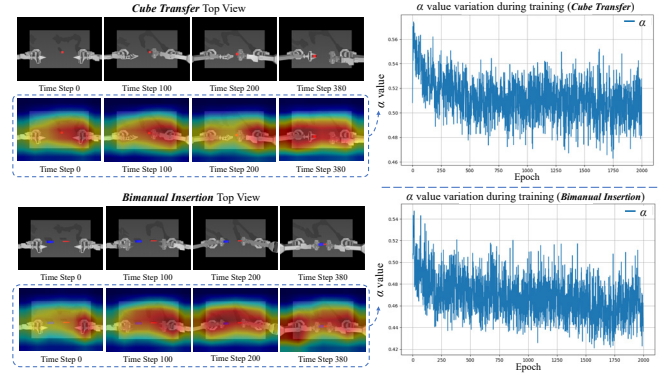


Fig. 6: Visualization of the dynamic weight α in the FE-EMA module (training phase, effect of 2000 epoch under different simulation tasks).

The Grad-CAM visualization technique qualitatively demonstrates the attention mechanism of the FE-EMA. For the qualitative analysis of the TS-DWT module, the attention of the frequency enhanced channels can be visualized. Compared to the output tensor of the Transformer encoder layer without TS-DWT integration, the FEWT framework is able to more significantly extract the importance of each channel dimension and the prominent features of different frequency components. The visualization of the frequency enhanced channel attention and the output tensor of the encoder layer on the Transformer are shown in **Fig. 7**.

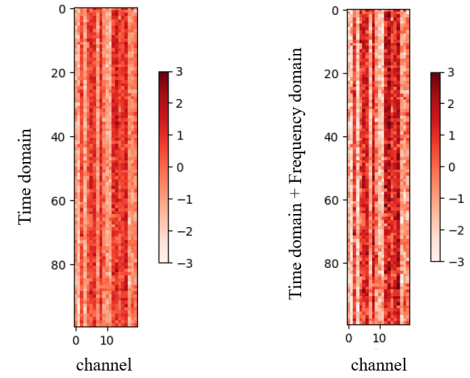


Fig. 7: Visualization of the frequency enhanced channel attention and the encoder layer's output tensor in the Transformer. x axis represents the channel dimension and y axis represents the frequency from low to high.

Finally, we evaluate algorithm performance in real-world humanoid robot tasks using success rate distributions from 50 tests, shown with violin and box plots. Each experiment was repeated 6 times to ensure reliability. Success rates are shown in **Fig. 8**, with ACT and FEWT medians annotated for clarity.

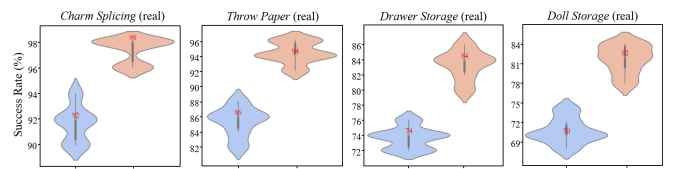


Fig. 8: Success rate comparison of algorithms in real-world humanoid robot tasks via violin and box plots.

V. CONCLUSION

The Humanoid Black Knight (HBK) hardware platform was designed for the deployment of learning algorithms in humanoid robots. Exoskeleton-style teleoperation for the collection of expert demonstration data allowed more anthropomorphic movement patterns, which facilitated natural manipulation. Perception representations of humanoid robots are enhanced through the FEWT framework. FEWT improves the success rate of the ACT baseline in simulation by up to 30% and by 6-12% in real-world mobile bimanual manipulation tasks. Currently, HBK has completed skill learning tests in localized scenarios. In the future, autonomous global skill learning will be achieved through hardware iteration and a lightweight design. By integrating multimodal perception sensors, such as radar, tactile sensors, and depth cameras, with a large language model, the perception accuracy and decision-making ability of the humanoid robot will be further enhanced. At the same time, by integrating reinforcement learning, we continue to explore robot policy learning for Sim2Real and extend it to the Real2Sim2Real paradigm, aiming to enhance the effective transfer and generalization between real and simulated environments.

REFERENCES

- [1] M. Zare, P. M. Kebria, A. Khosravi, and S. Nahavandi, "A Survey of Imitation Learning: Algorithms, Recent Developments, and Challenges," *IEEE Transactions on Cybernetics*, vol. 54, no. 12, pp. 7173-7186, 2024.
- [2] X. Chen, S. Xie, and K. He, "An empirical study of training self-supervised vision transformers," in *2021 IEEE/CVF International Conference on Computer Vision (ICCV)*, 2021, pp. 9640-9649.
- [3] K. Burns, Z. Witzel, J. I. Hamid, T. Yu, C. Finn, and K. Hausman, "What Makes Pre-Trained Visual Representations Successful for Robust Manipulation?," *arXiv preprint arXiv:2312.12444*, 2023.
- [4] D. Ouyang, S. He, G. Zhang, M. Luo, H. Guo, J. Zhan, and Z. Huang, "Efficient Multi-Scale Attention Module with Cross-Spatial Learning," in *2023 IEEE International Conference on Acoustics, Speech and Signal Processing (ICASSP)*, 2023, pp. 1-5.
- [5] K. He, X. Zhang, S. Ren, and J. Sun, "Deep residual learning for image recognition," in *2016 IEEE/CVF Conference on Computer Vision and Pattern Recognition (CVPR)*, 2016, pp. 770-778.
- [6] G. Xu, W. Liao, X. Zhang, C. Li, X. He, and X. Wu, "Haar wavelet downsampling: A simple but effective downsampling module for semantic segmentation," *Pattern Recognition*, vol. 143, p. 109819, 2023.
- [7] Y. Yang, G. Yuan, and J. Li, "SFFNet: A Wavelet-Based Spatial and Frequency Domain Fusion Network for Remote Sensing Segmentation," *IEEE Transactions on Geoscience and Remote Sensing*, vol. 62, pp. 1-17, 2024.
- [8] C. Zhao, W. Cai, C. Dong, and C. Hu, "Wavelet-based fourier information interaction with frequency diffusion adjustment for underwater image restoration," in *2024 IEEE/CVF Conference on Computer Vision and Pattern Recognition (CVPR)*, 2024, pp. 8281-8291.
- [9] M. Jiang, P. Zeng, K. Wang, H. Liu, W. Chen, and H. Liu, "FECAM: Frequency enhanced channel attention mechanism for time series forecasting," *Advanced Engineering Informatics*, vol. 58, p. 102158, 2023.
- [10] R. R. Selvaraju, M. Cogswell, A. Das, R. Vedantam, D. Parikh, and D. Batra, "Grad-cam: Visual explanations from deep networks via gradient-based localization," in *2017 IEEE/CVF International Conference on Computer Vision (ICCV)*, 2017, pp. 618-626.
- [11] T. Z. Zhao, V. Kumar, S. Levine, and C. Finn, "Learning fine-grained bimanual manipulation with low-cost hardware," in *RSS*, 2023.
- [12] E. Todorov, T. Erez, and Y. Tassa, "MuJoCo: A physics engine for model-based control," in *2012 IEEE/RSJ International Conference on Intelligent Robots and Systems (IROS)*, 2012, pp. 5026-5033.
- [13] A. Vaswani, *et al.*, "Attention is all you need," in *Conference on Neural Information Processing Systems (NeurIPS)*, 2017.
- [14] K. Darvish, *et al.*, "Teleoperation of Humanoid Robots: A Survey," *IEEE Transactions on Robotics*, vol. 39, no. 3, pp. 1706-1727, 2023.
- [15] A. Purushottam, Y. Jung, K. Murphy, D. Baek, and J. Ramos, "Hands-free Telelocomotion of a Wheeled Humanoid," in *2022 IEEE/RSJ International Conference on Intelligent Robots and Systems (IROS)*, 2022, pp. 8313-8320.
- [16] Z. Fu, T. Z. Zhao, and C. Finn, "Mobile ALOHA: Learning Bimanual Mobile Manipulation using Low-Cost Whole-Body Teleoperation," in *CoRL*, 2024.
- [17] Y. Liang, W. Li, Y. Wang, R. Xiong, Y. Mao, and J. Zhang, "Dynamic Movement Primitive based Motion Retargeting for Dual-Arm Sign Language Motions," in *2021 IEEE International Conference on Robotics and Automation (ICRA)*, 2021, pp. 8195-8201.
- [18] K. Ayusawa and E. Yoshida, "Motion Retargeting for Humanoid Robots Based on Simultaneous Morphing Parameter Identification and Motion Optimization," *IEEE Transactions on Robotics*, vol. 33, no. 6, pp. 1343-1357, 2017.
- [19] C. Chi, *et al.*, "Universal manipulation interface: In-the-wild robot teaching without in-the-wild robots," in *RSS*, 2024.
- [20] C. Zhou, L. Zhao, H. Wang, L. Chen, and Y. Zheng, "A Bilateral Dual-Arm Teleoperation Robot System with a Unified Control Architecture," in *2021 IEEE International Conference on Robot & Human Interactive Communication (RO-MAN)*, 2021, pp. 495-502.
- [21] M. Schwarz, C. Lenz, A. Rochow, M. Schreiber, and S. Behnke, "NimbRo Avatar: Interactive Immersive Telepresence with Force-Feedback Telemanipulation," in *2021 IEEE/RSJ International Conference on Intelligent Robots and Systems (IROS)*, 2021, pp. 5312-5319.
- [22] A. Iyer, *et al.*, "Open teach: A versatile teleoperation system for robotic manipulation," *arXiv preprint arXiv:2403.07870*, 2024.
- [23] A. Toedtheide, X. Chen, H. Sadeghian, A. Naceri, and S. Haddadin, "A Force-Sensitive Exoskeleton for Teleoperation: An Application in Elderly Care Robotics," in *2023 IEEE International Conference on Robotics and Automation (ICRA)*, 2023, pp. 12624-12630.
- [24] Y. Ishiguro, *et al.*, "Bilateral Humanoid Teleoperation System Using Whole-Body Exoskeleton Cockpit TABLIS," *IEEE Robotics and Automation Letters*, vol. 5, no. 4, pp. 6419-6426, 2020.
- [25] H. Fang, *et al.*, "AirExo: Low-Cost Exoskeletons for Learning Whole-Arm Manipulation in the Wild," in *2024 IEEE International Conference on Robotics and Automation (ICRA)*, 2024, pp. 15031-15038.
- [26] S. Yang, *et al.*, "ACE: A Cross-platform and visual-Exoskeletons System for Low-Cost Dexterous Teleoperation," in *CoRL*, 2024.
- [27] C. Chi, *et al.*, "Diffusion policy: Visuomotor policy learning via action diffusion," *The International Journal of Robotics Research*, p. 02783649241273668, 2023.
- [28] A. Gupta, S. Savarese, S. Ganguli, and L. Fei-Fei, "Embodied intelligence via learning and evolution," *Nature communications*, vol. 12, no. 1, p. 5721, 2021.
- [29] A. Brohan, *et al.*, "Rt-1: Robotics transformer for real-world control at scale," *arXiv preprint arXiv:2212.06817*, 2022.
- [30] B. Zitkovich, *et al.*, "Rt-2: Vision-language-action models transfer web knowledge to robotic control," in *CoRL*, 2023.
- [31] A. O'Neill, *et al.*, "Open X-Embodiment: Robotic Learning Datasets and RT-X Models : Open X-Embodiment Collaboration⁰," in *2024 IEEE International Conference on Robotics and Automation (ICRA)*, 2024, pp. 6892-6903.
- [32] J. Ho, A. Jain, and P. Abbeel, "Denoising diffusion probabilistic models," in *Conference on Neural Information Processing Systems (NeurIPS)*, vol. 33, pp. 6840-6851, 2020.
- [33] ViperX-300 6dof. in <https://www.trossenrobotics.com/viperx-300>.
- [34] D. Liu, F. Yang, X. Liao, and X. Lyu, "DIABLO: A 6-DoF Wheeled Bipedal Robot Composed Entirely of Direct-Drive Joints," in *2024 IEEE/RSJ International Conference on Intelligent Robots and Systems (IROS)*, 2024, pp. 3605-3612.